

## Observation of the Phononic Lamb Shift with a Synthetic Vacuum

T. Rentrop,<sup>1,\*</sup> A. Trautmann,<sup>1</sup> F. A. Olivares,<sup>1</sup> F. Jendrzejewski,<sup>1</sup> A. Komnik,<sup>2</sup> and M. K. Oberthaler<sup>1</sup>

<sup>1</sup>*Kirchhoff-Institut für Physik, Universität Heidelberg,  
Im Neuenheimer Feld 227, 69120 Heidelberg, Germany*

<sup>2</sup>*Institut für Theoretische Physik, Universität Heidelberg,  
Philosophenweg 12, 69120 Heidelberg, Germany*

(Received 8 July 2016; revised manuscript received 10 October 2016; published 28 November 2016)

In contrast to classical empty space, the quantum vacuum fundamentally alters the properties of embedded particles. This paradigm shift allows one to explain the discovery of the celebrated Lamb shift in the spectrum of the hydrogen atom. Here, we engineer a synthetic vacuum, building on the unique properties of ultracold atomic gas mixtures, offering the ability to switch between empty space and quantum vacuum. Using high-precision spectroscopy, we observe the phononic Lamb shift, an intriguing many-body effect originally conjectured in the context of solid-state physics. We find good agreement with theoretical predictions based on the Fröhlich model. Our observations establish this experimental platform as a new tool for precision benchmarking of open theoretical challenges, especially in the regime of strong coupling between the particles and the quantum vacuum.

DOI: [10.1103/PhysRevX.6.041041](https://doi.org/10.1103/PhysRevX.6.041041)

Subject Areas: Atomic and Molecular Physics,  
Quantum Physics

### I. INTRODUCTION

When an electron moves in the vacuum it drags a cloud of virtual photons with it [1]. As a result, its mass effectively increases. Since the coupling between the electron and the electromagnetic field cannot be switched off, it is impossible to observe the “bare” electron mass directly. An observable effect exists for the bound electron leading to a shift of the electronic energy levels in the hydrogen atom, known as the Lamb shift [2–5]. Similar effects take place in semiconductors where electrons couple to phononic excitations [6,7], leading to a quasiparticle known as a polaron. In these systems, the increase of the effective mass has been observed [8]. However, a quantitative measurement of the predicted phononic Lamb shift [9,10], which is defined for an electron bound to a donor ion, is still missing. Progress is hindered by uncontrolled disorder effects in such solid-state systems [11].

Here, we realize a model system for such a phononic quantum vacuum based on a strongly imbalanced mixture of ultracold atomic gases. Imbalanced Fermi gases already allowed for the observation of the Fermi polaron [12–15] and direct measurement of its increased effective mass [15] via oscillations in a weak optical trap. To observe the phononic Lamb shift, we immerse the particles of the minority species in a weakly confined Bose-Einstein condensate (BEC),

which realizes the phononic vacuum. In analogy to the electron bound to a donor ion, we additionally localize the particles of the minority species in a tight optical trap. By removing the BEC this system allows for switching off the quantum vacuum and with that to directly compare the dressed particle to the bare one, a feature that does not exist in experimental tests of quantum electrodynamics (QED) [16,17] and semiconductor systems.

We observe the phononic Lamb shift directly by high-resolution spectroscopy of the two lowest energy levels of the bound particle employing motional Ramsey spectroscopy [18], which provides improved resolution compared to other previously demonstrated spectroscopic techniques [15,19–21]. In this method, we measure the relative energy shift of particles confined in an approximately harmonic potential by letting them oscillate. For weak confinement we expect a slow down of oscillations due to the increased effective mass, which is computed for free particles; see Fig. 1(a). However, the confinement effects go far beyond this simple effective mass concept and have to be explicitly taken into account. We term the deviation between these two corrections phononic Lamb shift. Importantly, it can even lead to an increase of oscillation frequency as observed in our experiment. For our weakly interacting system the phononic Lamb shift is well described within the Fröhlich model [22–25] and can be computed with well-controlled perturbative methods.

\*LambShift@matterwave.de

*Published by the American Physical Society under the terms of the Creative Commons Attribution 3.0 License. Further distribution of this work must maintain attribution to the author(s) and the published article's title, journal citation, and DOI.*

### II. EXPERIMENTAL SETUP

In our experiment, a BEC of about  $10^6$  sodium atoms and few  $10^3$  to several  $10^4$  lithium atoms are both trapped by the

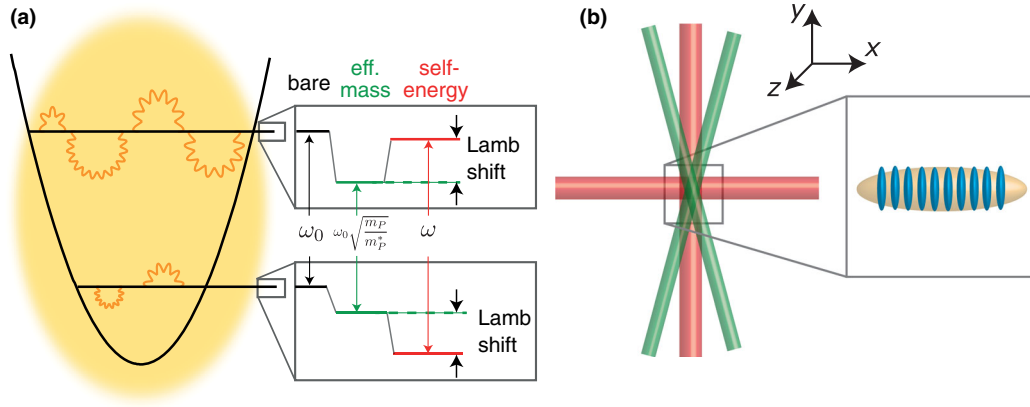


FIG. 1. Experimental setup. (a) Particles are trapped in a harmonic potential with trapping frequency  $\omega_0$ . The coupling of the particles to the quantum vacuum causes energy shifts of the particles' motional states. For a free particle, it leads to a mass increase, which would manifest itself to a smaller energy difference between the harmonic trap levels, as shown in the second column of the inset. For a trapped particle, the effective mass approximation breaks down and the energy shift has to be calculated from the self-energy in the confined geometry. The difference between the complete calculation and the effective mass approximation is termed phononic Lamb shift, and it can be so substantial that the interaction with the vacuum actually leads to an increased energy difference compared to the bare case, as shown in the third column of the inset. (b) Scheme of the experimental setup. The two atomic species are trapped in a single dipole trap (red beams). The lithium atoms, which act as the particles in this setup, experience additionally a strong confinement by a deep small-angle optical lattice (green beams), whose minima can be described by a harmonic potential with trapping frequency  $\omega_0$ . Inset: This setup results in a multitude of independent lithium clouds (blue) embedded in a large sodium Bose-Einstein condensate (yellow), which acts as the quantum vacuum.

same two beam optical dipole trap (ODT) at a wavelength of 1064 nm, as sketched in Fig. 1(b) [26]. The mean trapping frequency for  $^{23}\text{Na}$  is  $\bar{\omega} = 2\pi \times 150$  Hz. The temperature of the sample is about 350 nK. We can choose to work with fermionic  $^6\text{Li}$  as well as bosonic  $^7\text{Li}$  at mean trapping frequencies of  $\bar{\omega} = 2\pi \times 340$  Hz for  $^6\text{Li}$  and  $\bar{\omega} = 2\pi \times 310$  Hz for  $^7\text{Li}$ . The interspecies interaction strength is attractive for fermionic  $^6\text{Li}$  ( $a_{pV} = -75a_0$ ) [27] and repulsive for bosonic  $^7\text{Li}$  ( $a_{pV} = +21a_0$ ), with  $a_0$  being the Bohr radius. We use the subscript  $P$  for all quantities related to lithium particles, while the variables describing the quantum vacuum created by the sodium condensate carry the subscript  $V$ . The intraspecies interaction in Li is negligible, as fermions at low temperatures do not scatter and the intraspecies scattering length for the bosons is  $7a_0$  [28].

An additional optical lattice close to the D-line transitions for lithium ( $\lambda_{\text{res,Li}} \approx 671$  nm) imposes a very strong confinement in one direction for lithium. It consists of two intersecting laser beams, leading to a periodicity of  $d_{\text{lat}} = 1.65 \mu\text{m}$  and a typical depth of  $V_P/h \approx 78$  kHz for  $^6\text{Li}$  ( $V_P/h \approx 81$  kHz for  $^7\text{Li}$ ), where  $h$  is the Planck constant. This corresponds to an energy gap between the first and second energy band of  $\omega_0/2\pi = 27.3$  kHz for  $^6\text{Li}$  ( $\omega_0/2\pi = 26.2$  kHz for  $^7\text{Li}$ ). Because of the depth of the potential and the large lattice spacing, tunneling between lattice sites can be neglected and the minima can be treated as independent harmonic oscillators with trapping frequency  $\omega_0$ , resulting in multiple realizations of the experiment in a single experimental cycle.

Given the large detuning from the D-line transitions of sodium ( $\lambda_{\text{res,Na}} \approx 589$  nm), the depth of the optical lattice ( $V_V/h < 0.5$  kHz) is much weaker for this species and leads only to weak modulation of the BEC with a chemical potential of  $\mu_V/h \approx 5.5$  kHz.

### III. PHONONIC LAMB SHIFT FOR FERMIONIC PARTICLES

First, we discuss the case of fermionic  $^6\text{Li}$  particles in order to be as close as possible to the conventional Lamb shift. Our goal is the measurement of the energy difference  $\omega = E_1 - E_0$  between the particle energies in the ground and the first excited states of the harmonic oscillator. We perform the measurement both in the empty space, where the BEC is absent, and with the quantum vacuum in place. For the symmetric superposition of the ground and excited states,  $\omega$  can be extracted from the phase  $\phi = \omega t$  during a free evolution with duration  $t$ . This is the idea behind the motional Ramsey sequence we employ here [18].

After initial preparation in the ground state of the harmonic oscillator, we create a coherent superposition in the two lowest energy states of the harmonic oscillator by shaking the optical lattice. The resulting Rabi frequency is 1.4 kHz [29], and by coupling the states for 187  $\mu\text{s}$ , an equal superposition of ground and excited state is created ( $\pi/2$  pulse). Figure 2(b) shows a Rabi cycle, which we use for the calibration of the excited fraction  $\eta$ . In the subsequent time evolution, the excited motional state

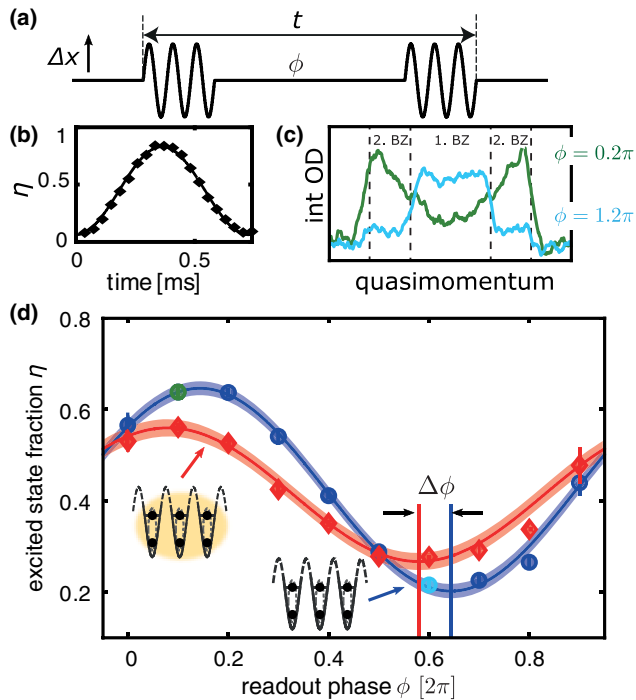


FIG. 2. Motional Ramsey spectroscopy. (a) The sequence of total time  $t$  consists of a  $\pi/2$  pulse creating an equal superposition between the ground and the excited state and a subsequent free evolution during which a phase  $\phi$  is accumulated. A second  $\pi/2$  pulse maps the phase shift on the population  $\eta$ . (b) Shaking the optical lattice couples the motional states of the lithium particles and allows the preparation of a superposition of the two lowest motional states. (c) Changing the evolution time  $t$  results in a Ramsey fringe in the population of the excited state, which is read out via band mapping on the first and second Brillouin zone. Typical optical density (OD) profiles of the resulting absorption images are depicted with a field of view of  $1176 \mu\text{m}$ . The dashed lines mark the limit of the Brillouin zones. (d) An exemplary interference fringe of  ${}^6\text{Li}$  after an evolution time of  $1.1 \text{ ms}$  is shown. The green and the blue dot correspond to the profiles that are presented above. In the case of an evolution with the BEC present, the amplitude is reduced due to dephasing and the fringe is shifted, showing an increased energy difference. The shaded area corresponds to the  $1\sigma$  confidence levels of the phase estimation.

accumulates a phase with respect to the ground state corresponding to its energy difference.

The accumulated phase difference can be mapped onto an observable population difference by applying an additional  $\pi/2$  pulse. In our system of periodically arranged harmonic oscillators, the population difference can be accessed by the band-mapping technique, where the quasimomentum in the lattice is mapped onto the free expansion of an atomic cloud [30–32]. While adiabatically reducing the lattice depth in  $2 \text{ ms}$  with a time constant  $\tau = 0.8 \text{ ms}$ , the longitudinal confinement through one beam of the ODT is turned off, allowing the atoms to expand in an optical waveguide along the lattice direction. After  $10 \text{ ms}$  of evolution an absorption image is taken. With

this technique a sufficient optical density can be obtained even for very low lithium atom numbers. To extract the population of the harmonic oscillator states, the absorption images are integrated transversally to the lattice direction, as shown in Fig. 2(c). In order to extract the relative occupation of the three lowest states, atoms in the areas of the three Brillouin zones are counted and the ratios are calculated.

The second pulse is shifted in time to record the phase of the oscillation [33], as shown in Fig. 2(d) (red curve). To measure the effect of the vacuum on the frequency, the sodium BEC is removed by a resonant light pulse before the Ramsey sequence starts. This light pulse does not have any observable effect on the Li sample. We clearly observe a fringe shift [Fig. 2(d), blue curve] in the absence of the BEC. The frequency change is given by  $\Delta\omega = \Delta\phi/\Delta t$ , where  $\Delta t$  is the total evolution time, including the time of the state coupling (pulses). The observed sign of the phase shift  $\Delta\phi$  corresponds to an increase of the energy difference.

For a quantitative comparison, care has to be taken since the employed near-resonance lattice for lithium also induces a weak modulation of the sodium BEC, as shown in the upper row of Fig. 3. In the Thomas-Fermi approximation, the modulation of the BEC density is  $\rho_{\text{mod}} = [\mu_V - V_V(x)]/g_V$ , with  $g_V = 4\pi\hbar^2 a_V/m_V$ , where  $\hbar = h/2\pi$ ,  $m_V$  is the mass of the sodium atoms, and  $a_V = 54.54a_0$  is the intraspecies scattering length [34]. It modifies the effective confinement of the minority species due to mean-field interactions between the two species. These interactions lead to the additional effective potential for the particles. The resulting potential for the lithium atoms is, therefore, a combination of the optical lattice and the modulated BEC,  $V_{P,\text{eff}}(x) = V_P(x) - g_{PV}\rho_{\text{mod}}$ , with  $g_{PV} = 2\pi\hbar^2 a_{PV}/m_r$ ,  $m_r$  is the reduced mass of the system; see, e.g., Refs. [23,35–37]. The band gap between the first and excited band in the effective potential is  $\omega_{\text{eff}}$ . Within the approximation that the sites are independent harmonic oscillators, the relative shift due to the lattice is then

$$\delta_{\text{latt}} = \frac{\omega_{\text{eff}} - \omega_0}{\omega_0} \approx -\frac{1}{2} \frac{g_{PV} V_V}{g_V V_P}. \quad (1)$$

These effects are isolated by performing the Ramsey spectroscopy at different detunings of the lattice, as shown in the lower left-hand panel of Fig. 3. While going closer to the lithium resonance, the potential depth  $V_P$  is kept constant by reducing the light intensity accordingly. Since the transition frequency for the background BEC is far detuned, the corresponding potential  $V_V$  is reduced and the modulation suppressed. We observe that the frequency shifts have a finite offset at the interpolated limit of zero modulation, which we denote with  $\delta_{\text{self}}$ . The fit yields for fermionic  ${}^6\text{Li}$  (blue dots) the relative shift

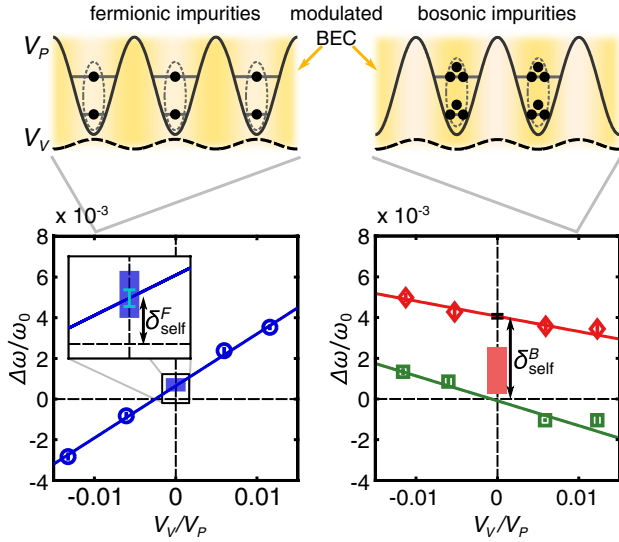


FIG. 3. Observation of the energy shift. The residual modulation of the density of the background BEC leads to an additional energy shift of the particle energy level. This can be identified by altering the ratio  $V_V/V_P$  through a change of the detuning of the optical lattice while keeping the potential depth for the particle constant. A clear linear dependence on  $V_V/V_P$  is observed. Interpolating the measurement data to  $V_V = 0$  allows for extraction of the energy shift. The positive offset is a direct signature of the phononic Lamb shift, since it contradicts the negative energy shift expected from the increased effective mass. The shaded areas show the theoretically predicted shift in the Fröhlich scenario, taking into account the uncertainties of the experimental parameters. We find perfect agreement without free parameters for fermionic particles (blue). In the case of a noncondensed bosonic particle cloud (green squares), no shift is observable in agreement with the theoretical expectation. For a condensed bosonic particle cloud (red diamonds), we observe a significant change of the energy shift. The theoretical expectation, not taking into account thermal excitations ( $T = 0$ ), is depicted as the red shaded area.

$\delta_{\text{self}}^F = 6.4(1.2) \times 10^{-4}$ , where the error bar corresponds to the 68% confidence interval.

This positive shift corresponds to an increase of the energy difference, which is at odds with a naive interpretation of an increased mass, and a more precise theoretical treatment including the phononic Lamb shift is necessary.

#### IV. THEORETICAL TREATMENT

A commonly used model describing strongly imbalanced mixtures is the celebrated Fröhlich Hamiltonian [23,24]:

$$H = H_P + H_V + H_{\text{Int}}, \quad (2)$$

where the individual components are given by

$$\begin{aligned} H_P &= \sum_k E_k \hat{a}_k^\dagger \hat{a}_k, \\ H_V &= \sum_q \omega_q \hat{b}_q^\dagger \hat{b}_q, \\ H_{\text{Int}} &= \sum_{k,q \neq 0} V_q \hat{a}_{k+q}^\dagger \hat{a}_k (\hat{b}_q + \hat{b}_{-q}^\dagger). \end{aligned} \quad (3)$$

$E_k$  represent the energy levels of the uncoupled particles.  $\omega_q = cq[1 + (\xi q)^2/2]^{1/2}$ , where  $c = \sqrt{g_V \rho_{\text{BEC}}/m_V}$  is the speed of sound, describes the dispersion relation of the excitations to the quantum vacuum. The particle (vacuum excitation) creation and annihilation operators are denoted  $\hat{a}_k^\dagger$  ( $\hat{b}_q^\dagger$ ) and  $\hat{a}_k$  ( $\hat{b}_q$ ). The third term arises from the density-density interaction between the particles and the BEC. It describes the change in momentum of the particle via the absorption or emission of a phonon. We emphasize that the coupling strength  $V_q$  captures the contact interaction in our system, which is different from the long-range Coulomb interaction of an electron in a semiconductor and which is given by

$$V_{\mathbf{q}} = g_{PV} \sqrt{\rho_{\text{BEC}}} \{(\xi q)^2 / [(\xi q)^2 + 2]\}^{1/4}, \quad (4)$$

where  $\xi = (8\pi\rho_{\text{BEC}}a_V)^{-1/2}$  is the healing length of the condensate. Given the varying density  $\rho_{\text{BEC}}$  in the trap  $\xi$  varies and has to be recalculated for each specific case, but it is typically on the order of  $0.5 \mu\text{m}$ . In the case of weak interactions, when the interaction parameter,

$$\alpha = \frac{a_{PV}^2}{\xi a_V} = \frac{m_r^2 E_{PV}^2}{\pi m_V^2 E_{\text{ph}}^2}, \quad (5)$$

is much smaller than unity,  $\alpha \ll 1$ , the particle-phonon interaction term allows for perturbative treatment. Here, we introduce the characteristic energy scale for particle-phonon interaction,  $E_{PV} = g_{PV} \sqrt{\rho_{\text{BEC}}} \xi^{-3}$ , and the characteristic energy of the phonons,  $E_{\text{ph}} = (\hbar c/\xi)$ . So, according to Refs. [23,38],  $\alpha \ll 1$  simply states that the coupling should be small enough to avoid the quantum depletion of the condensate.

The canonical interpretation of the lowest-order correction to the particle dispersion is that of an enhanced effective mass  $m_p^* > m_p$ . Following the lines of Ref. [39] by calculating the lowest-order self-energy diagram (on shell) and computing its derivative with respect to squared momentum, we find  $m_p^*/m_p = 1 + \nu\alpha + \dots$ , where  $\nu \approx 0.364$  and  $0.336$  for  ${}^6\text{Li}$  and  ${}^7\text{Li}$  setups, respectively. These are the results for the unconstrained system, when there is no confinement potential for both the BEC as well as the particles. Should the fermions be confined in a harmonic potential with frequency  $\omega_0$ , then a naive expectation for the shift of the energy levels is  $\omega_0 \rightarrow \omega_0(1 - \nu\alpha/2 + \dots)$ . This entails a downward energy level shift corresponding to a slow down of the oscillations

and growing with the primary quantum number [40]; see Fig. 1(a).

This is not supported by the experimental evidence, and one must improve the model. In order to include this effect, we take care of the system's geometry by modifying the Hamiltonian Eq. (2). From now on, we consider the particles as being confined in a parabolic potential (energy parameter  $\hbar\omega_0$  and length parameter  $a_{\text{HO}} = \sqrt{\hbar/m_p\omega_0} \approx 0.24 \mu\text{m}$ ) in the  $x$  direction, and being free in all other spatial dimensions. Their eigenstates then have energies  $E_{n,\mathbf{k}} = \hbar\omega_0(n + 1/2) + \hbar^2 k^2/2m_p - \mu$ , where  $\mathbf{k}$  is a 2D wave vector and  $n$  denotes the respective principal quantum number for the particles in the confinement potential. The unperturbed particle Hamiltonian is then

$$H_P = \sum_n \int \frac{d^2\mathbf{k}}{(2\pi)^2} E_{n,\mathbf{k}} \hat{a}_{n,\mathbf{k}}^\dagger \hat{a}_{n,\mathbf{k}}. \quad (6)$$

Adapting the interaction term to the present setup leads to the following expression:

$$H_{\text{Int}} = \int \frac{d^2\mathbf{k}}{(2\pi)^2} \int \frac{d^3\mathbf{q}}{(2\pi)^3} \sum_{n_1, n_2} V_{\mathbf{q}} A(n_1, n_2, q_x) \times \hat{a}_{n_1, \mathbf{k}+\mathbf{q}}^\dagger \hat{a}_{n_2, \mathbf{k}} (\hat{b}_{\mathbf{q}} + \hat{b}_{-\mathbf{q}}^\dagger). \quad (7)$$

Here,  $\mathbf{q}' = (q_y, q_z)$  denotes the transverse component of the phonon momentum.  $A$  is the matrix element for the transition between the harmonic oscillator energy levels:

$$A(n_1, n_2, q_x) = \int dx \varphi_{n_1}^*(x) \varphi_{n_2}(x) e^{-iq_x x}, \quad (8)$$

$$\Sigma(n, \mathbf{k}; i\Omega) = \frac{ig_{PV}^2 \rho_{\text{BEC}}}{\beta} \int \frac{d^3\mathbf{q}}{(2\pi)^3} \sum_{i\epsilon_j} \sqrt{\frac{(\xi q)^2}{(\xi q)^2 + 2}} \sum_{m=0}^{\infty} A^*(n, m, q_x) A(m, n, q_x) G[m, \mathbf{k} - \mathbf{q}', i\Omega - (m-n)\omega_0 - i\epsilon_j] D_0(i\epsilon_j, \mathbf{q}), \quad (11)$$

where  $\Omega$  is a particle and  $\epsilon_j = 2\pi j/\beta$  bosonic (phonons) Matsubara frequencies.  $\beta = 1/k_B T$  is the inverse temperature, where  $k_B$  is the Boltzmann constant, and  $\rho_{\text{BEC}}$  is the density of the sodium BEC. The necessary Green functions are

$$D_0(i\epsilon_j, \mathbf{q}) = \frac{2\omega_{\mathbf{q}}}{(i\epsilon_j)^2 - \omega_{\mathbf{q}}^2}, \quad (12)$$

$$G[m, \mathbf{k} - \mathbf{q}', i\Omega - (m-n)\omega_0 - i\epsilon_j] = \frac{1}{i\Omega - (m-n)\omega_0 - i\epsilon_j - E_{m, \mathbf{k}-\mathbf{q}'}}}, \quad (13)$$

where  $D_0$  and  $G$  are the phonon and the particle Green function, respectively.  $G$  has the same shape for both

where  $\varphi_n(x)$  are the wave functions of the  $n$ th eigenstate. Finally, the Hamiltonian of the phonons is a continuum version of Eq. (3):

$$H_V = \int \frac{d^3\mathbf{q}}{(2\pi)^3} \omega_{\mathbf{q}} \hat{b}_{\mathbf{q}}^\dagger \hat{b}_{\mathbf{q}}. \quad (9)$$

Matrix elements for the particle-phonon scattering are still given by Eq. (4).

Here, the dimensionless interaction parameter is modified as compared to the free unconstrained system [see Eq. (5)]:

$$\alpha_{\text{con}} = \frac{g_{PV}^2 \rho_{\text{BEC}} m_V}{8\pi^2 \hbar^3 \omega_0 \xi} = \frac{1}{\sqrt{2} 8\pi^2} \frac{E_{PV}^2}{E_{\text{Ph}} \hbar \omega_0}. \quad (10)$$

It can be interpreted as the ratio between the energy shift of the dressed states and the energy spacing of the bare states. For our experimental parameters,  $\alpha_{\text{con}} \approx 10^{-4}$ , which justifies a perturbative treatment also in the confined case.

Our goal is the energy level renormalization for the particles in the confinement potential. Just as in the case of the effective mass, its computation is best accomplished via lowest-order irreducible self-energy correction, which is, in general, different for different oscillator states  $n$ . The energy level structure is given by the retarded self-energy, which is computed via analytical continuation of its Matsubara counterpart, see, e.g., Ref. [39],

fermionic as well as bosonic particles. Performing the calculation in the assumption that only the two lowest-lying energy levels of the confining potential are equally populated, we compute their shifts due to interactions, which we call self-energy shifts, and subsequently extract the energy difference  $\delta_{\text{self}}$  between them. We take into account the Fermi distribution of the particles and find that in the relevant particle density region the energy shifts are only weakly dependent on the particles' chemical potential  $\mu$  and the ratio  $a_{\text{HO}}/\xi$ , which is typically on the order of 1, having the general form

$$\delta_{\text{self}} = \frac{\Delta\omega}{\omega_0} = \alpha_{\text{con}} f(\mu, a_{\text{HO}}, \xi, \eta), \quad (14)$$

where  $f(\mu, a_{\text{HO}}, \xi, \eta)$  is a dimensionless factor, an explicit expression for this quantity is bulky and can be evaluated only numerically. We stress that, in general, the function  $f$  explicitly depends on the population imbalance  $\eta$  between the ground and excited states of the confinement potential. Assuming  $T = 0$ , taking the actual experimental parameters in the case of symmetric superposition (when both oscillator states are equally populated), we obtain (for details see the Appendix)

$$f(\mu, a_{\text{HO}}, \xi, \eta = 1/2) = -0.11 + \frac{0.94}{a_{\text{HO}}/\xi}. \quad (15)$$

Using this result we can calculate the expectation value of the density-dependent phase shift at each point in the cloud. The band-mapping technique then yields the spatially averaged phase shift  $\Delta\phi$ . However, different parts of the lithium cloud are embedded in varying sodium densities, which leads to locally varying phase shifts,  $\phi(\mathbf{r}) = \omega_0 \delta_{\text{self}}(\mathbf{r})t$ . The coupling of the lithium particles to the large number of phononic modes is sufficiently strong that it leads to observable loss of visibility, through the dephasing of the different modes, during the Ramsey sequence and, therefore, limits the resolution. It can be taken into account via a position-dependent relaxation rate  $\Gamma(\mathbf{r})$ , which was studied in detail in Ref. [18]. The total signal of the fermions is then given by

$$\Delta\phi_F = \text{asin}\left(\frac{\int d^3\mathbf{r}\rho_{\text{Li}}(\mathbf{r})e^{-\Gamma(\mathbf{r})t} \sin[\phi(\mathbf{r})]}{\int d^3\mathbf{r}\rho_{\text{Li}}(\mathbf{r})e^{-\Gamma(\mathbf{r})t}}\right). \quad (16)$$

The density distributions are obtained numerically by taking into account the finite temperature as well as the external potentials, such as the optical lattice and the harmonic trapping due to the ODT. For lithium it is necessary to include the additional potential due to the interaction with sodium. We can then calculate the fringe shift according to Eq. (16), as shown by the shaded inset in Fig. 3, left-hand panel. The predicted phase shift is in very good agreement with our measurements.

The conventional notion of the Lamb shift is the energy difference between the  $s$  and  $p$  electron states in a hydrogen atom. It is, however, computed with the renormalized electron mass as the coupling amplitude of the quantum electrodynamics (fine-structure constant) cannot be switched off. According to this orthodox picture, the *true* Lamb shift in our system thus amounts to the energy difference between the shift due to the effective mass increase and the self-energy shift for confined particles; see Fig. 1(a). A direct measurement of the effective mass for particles in a phononic vacuum along the lines of Ref. [15] could help to clarify this subtlety. However, this important point is often ignored in the solid-state and semiconductor context, and the term Lamb shift is generally used to

describe energy level corrections of confined particles coupled to phonon continua.

## V. PHONONIC LAMB SHIFT FOR BOSONIC PARTICLES

Our new experimental platform further allows us to investigate the phononic Lamb shift with bosonic particles, a feature not available in other experiments. Calculating the phononic Lamb shift now for bosonic particles at  $T = 0$  leads to

$$\delta_{\text{self}} = \frac{\Delta\omega}{\omega_0} = \alpha_{\text{con}} f(\rho_{2\text{D}}, a_{\text{HO}}, \xi, \eta), \quad (17)$$

$$f(\rho_{2\text{D}}, a_{\text{HO}}, \xi, \eta) = \rho_{2\text{D}} \xi^2 [g_g(a_{\text{HO}}/\xi)(1-\eta) - g_e(a_{\text{HO}}/\xi)\eta], \quad (18)$$

$$g_g(a_{\text{HO}}/\xi) = \frac{8\pi^2}{\sqrt{2}} e^{(a_{\text{HO}}/\xi)^2} [1 - \text{erf}(a_{\text{HO}}/\xi)], \quad (19)$$

$$g_e(a_{\text{HO}}/\xi) = 4\pi \frac{a_{\text{HO}}}{\xi} \sqrt{2\pi} \times \left\{ 1 - \sqrt{\pi} \frac{a_{\text{HO}}}{\xi} e^{(a_{\text{HO}}/\xi)^2} [1 - \text{erf}(a_{\text{HO}}/\xi)] \right\}. \quad (20)$$

A crucial difference from the fermionic case is the explicit occurrence of the two-dimensional density of condensed particles  $\rho_{2\text{D}}$  in Eq. (18). The physical reason is that the condensed particles populate a single state and thus coherently scatter the phonons, leading to an amplification of the signal. Employing bosonic particles thus results in a larger Lamb shift due to bosonic enhancement.

We use this feature to boost the Lamb shift in experiments with bosonic particles ( $^7\text{Li}$ ) that are condensed ( $\approx 60\%$  condensate fraction). The results (red diamonds) are displayed in Fig. 3. We observe that the effect of the modulation of the background BEC is inverted and smaller than for fermionic particles, as the interspecies scattering length changes sign and is reduced by a factor of 3. Thus, the energy shift for a single boson is predicted to be 10 times smaller than for fermionic  $^6\text{Li}$ . Nevertheless, the observed energy shift is amplified by a few thousands of bosons in the ground state of each pancake, leading to  $\delta_{\text{self}}^B = 4.1(1) \times 10^{-3}$ . For comparison, we also perform the same experiments with a noncondensed cloud of  $^7\text{Li}$  atoms (green squares) at a temperature of  $\approx 450$  nK, leading to smaller numbers of atoms per quantum state, and a weakened coupling as we operated at an approximately 2 times smaller BEC density. As expected from the theoretical predictions, we do not observe any shift in this regime.

The observed total phase shift for the condensed particles can then be calculated from Eq. (17) as a lithium density weighted mean:

$$\Delta\phi_B = \text{asin}\left(\frac{\int d^3\mathbf{r}\rho_{\text{Li,BEC}}(\mathbf{r})\sin[\phi(\mathbf{r})]}{\int d^3\mathbf{r}\rho_{\text{Li,BEC}}(\mathbf{r})}\right). \quad (21)$$

Here, we assume that only the condensed part experiences an energy shift, as the thermal part will not experience the Bose amplification and the phononic Lamb shift is therefore negligible. However, the total signal is given as a weighted sum over shifted and unshifted phase patterns. The weak interaction between the BEC and the bosonic particles leads to long coherence times ( $\tau > 50$  ms), which are much longer than the Ramsey sequence, such that decoherence can be neglected in this case. In order to capture properly the lithium occupation number in the individual sites, we slice the ODT density according to the periodicity of the lattice. These occupation numbers enter the detailed calculation of the density distribution in the total confinement potential, where a 2D description is applied, and  $\rho_{2D}$  is obtained for each pancake individually.

The theoretically predicted phase shift is shown by the red shaded area in the right-hand panel of Fig. 3. It is much smaller than the observed shift. However, a quantitative comparison between theory and experiment is difficult in this specific case. The overlap between the two species is much more sensitive to details in the trap geometries, limiting its control. For the fermionic  $^6\text{Li}$ , Pauli blocking stabilizes the density distribution and the attractive interactions with the condensate lead to a large overlap between the two clouds. On the other hand, in the bosonic case, the condensation dramatically changes the density profile for temperatures of the order of the critical one. Further, the repulsive interactions between the bosonic  $^7\text{Li}$  and the condensate push the minority species to the edge of the sample, where the finite-temperature effects are most pronounced. This poses a challenge to the theoretical description. In addition, despite the fact that the interparticle interaction is very weak, we cannot exclude its contribution to the discrepancy.

For a more quantitative comparison between theory and experiment for bosonic particles, we measure the energy shift as a function of different populations of ground and excited state. Since the energy shift is proportional to the occupation number for bosons, there exists a specific relative population  $\eta_0$ , where the energy shifts are equal for both levels. Mathematically it corresponds to the point where  $f(\rho_{2D}, a_{\text{HO}}, \xi, \eta_0) = 0$ . For our experimental setup, this implies a vanishing phase shift for  $\eta_{0,\text{theor}} = 0.85(2)$ , where the uncertainty arises from the determination of the density profile. We emphasize that this crossing point depends only weakly on the overlap between the particles and the BEC. As such, it puts the theoretical predictions to a precise test.

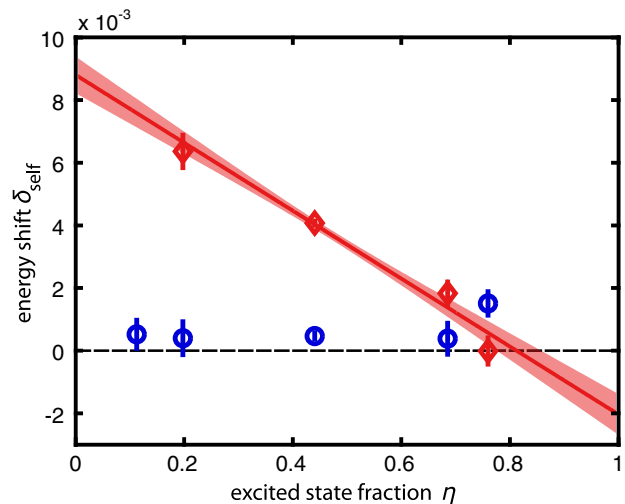


FIG. 4. Population dependence of the energy shift. The energy shift depends on the relative state population  $\eta$  as ground and excited state experience different energy shifts. This can be observed in a Ramsey sequence with an unequal superposition during free time evolution, keeping the other relevant parameters constant. Experiments with bosonic particles are shown by red diamonds. From these data we extract a critical  $\eta_{0,\text{expt}} = 0.81(7)$ , in good agreement with theoretical predictions of  $\eta_{0,\text{theor}} = 0.85(2)$ . For fermionic particles (blue circles) we do not observe any dependence on  $\eta$ , as expected from our calculations.

By varying the length of the first Ramsey pulse, the relative occupation of the excited state during time evolution is changed. Figure 4 depicts the dependence of  $\delta_{\text{self}}$  on the excited fraction and confirms the prediction [42]. The experiments with fermions (blue) do not reveal any significant change. This is in agreement with the theoretical analysis of the result [Eq. (14)], which reveals only weak dependence on  $\eta$  below the experimental sensitivity of our setup. In contrast, the data with bosonic particles (red) show a clear linear dependence in agreement with the theoretical prediction of Eq. (18). Motivated by this observation, we extract the crossing point via a linear fit, where the slope and the offset are left as free parameters. The observed crossing point at  $\eta_{0,\text{expt}} = 0.81(7)$  is in excellent agreement with the theoretical prediction. This observation confirms our understanding of the phononic Lamb shift for bosonic particles within the developed frameworks. It also suggests that the disagreement in the amplitude of the phononic Lamb shift might be due to uncontrolled systematic shifts in the overlap between the BEC and the lithium particles, which should be investigated in future works.

## VI. CONCLUSION

Our results are in the realm of implementation of analog quantum simulators on the basis of ultracold gas mixtures [32,43]. We open up an avenue for benchmarking a new class of many-body theories, comprising not only different mutually interacting particles, but also interactions of their

collective excitations. Such models are, e.g., proposed to play a decisive role in fundamental open problems as the origin of the high-temperature superconductivity; see Ref. [44]. Furthermore, this setup captures several important nonrelativistic features of QED. In this way, we realize a new experimental platform for quantitative exploration of such fascinating phenomena such as Casimir effect in low-dimensional systems, where quantum fluctuations are dramatically enhanced [45,46], as well as in dynamical situations [47–49]. By varying the distance between the lattice valleys, we could directly test the dependence of the energy shift on this spacing and therefore measure sign and amplitude of the vacuum-induced forces. In a many-particle limit, the background-mediated interaction between the particles can also lead to a generation and detection of nonlocal entanglement [50].

### ACKNOWLEDGMENTS

We would like to thank F. Grusdt, E. Demler, and R. Schmidt for discussions. This work was supported by the Heidelberg Center for Quantum Dynamics, the

ExtreMe Matter Institute, and the European Commission FET-Proactive grant AQUs (Project No. 640800). This work is part of and supported by the DFG Collaborative Research Centre “SFB 1225 (ISOQUANT)”. F. A. O. acknowledges support by the IMPRS-QD. A. K. is supported by the Heisenberg Programme of the Deutsche Forschungsgemeinschaft (Germany) under Grant No. KO 2235/5-1.

*Note added.*—Recently, we became aware of the recent observation of the Bose polaron in the strong coupling limit in the vicinity of a Feshbach resonance [51,52].

### APPENDIX: DETAILS OF THE CALCULATIONS

Here, we present the details of the calculations in the fermionic case. First, we can compute the sum over the Matsubara frequencies  $\epsilon_j$  in Eq. (11) and perform the analytic continuation procedure  $i\Omega \rightarrow \omega + i\delta$  in order to obtain the retarded self-energy ( $\delta$  is a positive infinitesimal):

$$\begin{aligned} \Sigma(n, \mathbf{k}; \omega) = & -g_{PV}^2 \rho_{\text{BEC}} \int \frac{d^3 \mathbf{q}}{(2\pi)^3} \sqrt{\frac{(\xi q)^2}{(\xi q)^2 + 2}} \sum_{m=0}^{\infty} A^*(n, m, q_x) A(m, n, q_x) \\ & \times \left( \frac{N_{\mathbf{q}} + n_F}{\omega - (m-n)\omega_0 - E_{m, \mathbf{k}-\mathbf{q}'} + \omega_{\mathbf{q}} + i\delta} + \frac{N_{\mathbf{q}} + 1 - n_F}{\omega - (m-n)\omega_0 - E_{m, \mathbf{k}-\mathbf{q}'} - \omega_{\mathbf{q}} + i\delta} \right), \end{aligned}$$

where  $n_F$  is the Fermi distribution function of particles and  $N_{\mathbf{q}} = 1/[\exp(\beta\omega_{\mathbf{q}}) - 1]$  stands for the Bose distribution of phonons. For the particles in the ground state of the confinement potential  $n = 0$ , there two classes of processes: scatterings within the  $n = 0$  state and scatterings into the first excited state  $m = 1$ . The corresponding terms are very similar and we exemplarily show the computations due to the first kind of transitions. In the above result it is convenient to go over to an integral over  $s = |\mathbf{k} - \mathbf{q}'|$  and over the angle  $\theta$  between the vectors  $\mathbf{k}$  and  $\mathbf{q}'$ . After performing the latter, we obtain

$$\Sigma_{00}(\mathbf{k}; \omega) = \frac{g_{PV}^2 \rho_{\text{BEC}}}{8\pi^2 k} \int dq_x dq' \sqrt{\frac{(\xi q)^2}{(\xi q)^2 + 2}} e^{-(a_{\text{HO}} q_x)^2 / 2} \int_{|k-q'|}^{k+q'} ds s \left( \frac{N_{\mathbf{q}} + n_F(s)}{\omega - E_{0,s} + \omega_{\mathbf{q}} + i\delta} + \frac{N_{\mathbf{q}} + 1 - n_F(s)}{\omega - E_{0,s} - \omega_{\mathbf{q}} + i\delta} \right), \quad (\text{A1})$$

where the subscript 00 reflects the fact that we consider particle scatterings within the ground state of the harmonic oscillator. In the next step, we use the Plemelj formula in order to split off the real part of the self-energy yielding the energy shift. This procedure formally amounts to taking the principal value of the above integrals in the limit  $\delta \rightarrow 0$ . Then the energy correction for the particle with the energy  $\omega = k^2/2m_P$  takes the following form:

$$\begin{aligned} \delta\epsilon_{00} = & \frac{g_{PV}^2 \rho_{\text{BEC}} m_P}{8\pi^2 \hbar^2 \xi \kappa} \int d\eta_x d\eta' \sqrt{\frac{\eta'^2 + \eta_x^2}{\eta'^2 + \eta_x^2 + 2}} e^{-(a_{\text{HO}}/\xi)^2 \eta_x^2 / 2} \\ & \times \int_{(\kappa-\eta')^2}^{(\kappa+\eta')^2} d\epsilon \left( \frac{N_{\mathbf{q}} + n_F(\epsilon)}{\kappa^2 - \epsilon + Y \sqrt{\eta'^2 + \eta_x^2} \sqrt{1 + (\eta'^2 + \eta_x^2)/2}} + \frac{N_{\mathbf{q}} + 1 - n_F(\epsilon)}{\kappa^2 - \epsilon - Y \sqrt{\eta'^2 + \eta_x^2} \sqrt{1 + (\eta'^2 + \eta_x^2)/2}} \right), \quad (\text{A2}) \end{aligned}$$

where the integrals are over dimensionless variables  $\eta' = q'\xi$ ,  $\eta_x = q_x\xi$ ,  $\kappa = k\xi$ , and  $Y = \sqrt{2}m_P/m_V$ . Here, one has to keep in mind that the fermionic chemical potential  $\mu$  is now measured in units of  $\hbar^2/(2m_P\xi^2)$ . The remaining integrals can be evaluated only numerically. The result depends on  $\mu 2m_P\xi^2/\hbar^2$  (which is ultimately related to the band imbalance parameter  $\eta$ ; see main text), the ratio  $a_{\text{HO}}/\xi$ , and  $\kappa$ . It turns out that, in the relevant experimental parameter regime ( $T = 0$  and numbers

given in the main text), the integral is to a good degree of accuracy linear in  $\kappa$ , canceling the  $\sim 1/\kappa$  prefactor. In a similar way, one can obtain the expressions for the energy shifts for particles in the harmonic oscillator ground state due to their excursions into the first excited states  $\delta\epsilon_{01}$  as well as the shifts for the particles residing in the first excited state  $\delta\epsilon_{10}$  and  $\delta\epsilon_{11}$ . The differences from Eq. (A1) are only the matrix elements  $A(n, m, q_x)$  [see Eq. (8)], which lead to the extension of the exponential factor  $e^{-(a_{\text{HO}}q_x)^2/2}$  by  $(a_{\text{HO}}q_x)^2/2$  and  $[1 - (a_{\text{HO}}q_x)^2]/4$ , respectively. In addition, in the energy denominators of Eq. (A1) there is a trivial adjustment of energies by  $\omega_0$  for the terms corresponding to scatterings into the adjacent level of the confinement potential. Combining all corrections to the energy difference between the lowest two states of the confinement potential and normalizing to  $\omega_0$ , we obtain the result Eq. (14), where the function  $f(\mu, a_{\text{HO}}, \xi, \eta)$  for the actual experimental setup is given in Eq. (15).

Following the same line, one performs the calculation for the bosonic particles.

- 
- [1] P. W. Milonni, *The Quantum Vacuum: An Introduction to Quantum Electrodynamics* (Academic Press, Boston, 1994).
- [2] W. Lamb and R. Retherford, *Fine Structure of the Hydrogen Atom by a Microwave Method*, *Phys. Rev.* **72**, 241 (1947).
- [3] H. A. Bethe, *The Electromagnetic Shift of Energy Levels*, *Phys. Rev.* **72**, 339 (1947).
- [4] D. J. Berkeland, E. A. Hinds, and M. G. Boshier, *Precise Optical Measurement of Lamb Shifts in Atomic Hydrogen*, *Phys. Rev. Lett.* **75**, 2470 (1995).
- [5] M. Niering, R. Holzwarth, J. Reichert, P. Pokasov, Th. Udem, M. Weitz, T. W. Hänsch, P. Lemonde, G. Santarelli, M. Abgrall, P. Laurent, C. Salomon, and A. Clairon, *Measurement of the Hydrogen 1S – 2S Transition Frequency by Phase Coherent Comparison with a Microwave Cesium Fountain Clock*, *Phys. Rev. Lett.* **84**, 5496 (2000).
- [6] L. D. Landau, *Phys. Z. Sowjetunion* **3**, 664 (1933); *electron motion in crystal lattices*, in *Collected Papers of L.D. Landau*, edited by D. T. Haar, 1965, ISBN .
- [7] R. P. Feynman, *Slow Electrons in a Polar Crystal*, *Phys. Rev.* **97**, 660 (1955).
- [8] J. W. Hodby, T. E. Jenkins, C. Schwab, H. Tamura, and D. Trivich, *Cyclotron Resonance of Electrons and of Holes in Cuprous Oxide, Cu<sub>2</sub>O*, *J. Phys. C* **9**, 1429 (1976).
- [9] P. M. Platzman, *Ground-State Energy of Bound Polarons*, *Phys. Rev.* **125**, 1961 (1962).
- [10] T. K. Mitra, A. Chatterjee, and S. Mukhopadhyay, *Polarons*, *Phys. Rep.* **153**, 91 (1987).
- [11] P. E. Simmonds, J. M. Chamberlain, R. A. Hoult, R. A. Stradling, and C. C. Bradley, *Far-Infrared Spectroscopy of Bound and Free Electrons in III-V and II-VI Semiconductors. I. Transitions between Excited States Observed in Zeeman Spectroscopy of the Shallow Donor Impurities*, *J. Phys. C* **7**, 4164 (1974).
- [12] M. Koschorreck, D. Pertot, E. Vogt, B. Fröhlich, M. Feld, and M. Köhl, *Attractive and Repulsive Fermi Polarons in Two Dimensions*, *Nature (London)* **485**, 619 (2012).
- [13] C. Kohstall, M. Zaccanti, M. Jag, A. Trenkwalder, P. Massignan, G. M. Bruun, F. Schreck, and R. Grimm, *Metastability and Coherence of Repulsive Polarons in a Strongly Interacting Fermi Mixture*, *Nature (London)* **485**, 615 (2012).
- [14] A. Schirotzek, C. H. Wu, A. Sommer, and M. W. Zwierlein, *Observation of Fermi Polarons in a Tunable Fermi Liquid of Ultracold Atoms*, *Phys. Rev. Lett.* **102**, 230402 (2009).
- [15] S. Nascimbène, N. Navon, K. J. Jiang, L. Tarruell, M. Teichmann, J. McKeever, F. Chevy, and C. Salomon, *Collective Oscillations of an Imbalanced Fermi Gas: Axial Compression Modes and Polaron Effective Mass*, *Phys. Rev. Lett.* **103**, 170402 (2009).
- [16] M. Brune, P. Nussenzweig, F. Schmidt-Kaler, F. Bernardot, A. Maali, J. M. Raimond, and S. Haroche, *From Lamb Shift to Light Shifts: Vacuum and Subphoton Cavity Fields Measured by Atomic Phase Sensitive Detection*, *Phys. Rev. Lett.* **72**, 3339 (1994).
- [17] A. Fragner, M. Göppl, J. M. Fink, M. Baur, R. Bianchetti, P. J. Leek, A. Blais, and A. Wallraff, *Resolving Vacuum Fluctuations in an Electrical Circuit by Measuring the Lamb Shift*, *Science* **322**, 1357 (2008).
- [18] R. Scelle, T. Rentrop, A. Trautmann, T. Schuster, and M. K. Oberthaler, *Motional Coherence of Fermions Immersed in a Bose Gas*, *Phys. Rev. Lett.* **111**, 070401 (2013).
- [19] S. Will, T. Best, S. Braun, U. Schneider, and I. Bloch, *Coherent Interaction of a Single Fermion with a Small Bosonic Field*, *Phys. Rev. Lett.* **106**, 115305 (2011).
- [20] J. Heinze, S. Götze, J. S. Krauser, B. Hundt, N. Fläschner, D. S. Lühmann, C. Becker, and K. Sengstock, *Multiband Spectroscopy of Ultracold Fermions: Observation of Reduced Tunneling in Attractive Bose-Fermi Mixtures*, *Phys. Rev. Lett.* **107**, 135303 (2011).
- [21] J. Catani, G. Lamporesi, D. Naik, M. Gring, M. Inguscio, F. Minardi, A. Kantian, and T. Giamarchi, *Quantum Dynamics of Impurities in a One-Dimensional Bose Gas*, *Phys. Rev. A* **85**, 023623 (2012).
- [22] H. Fröhlich, *Electrons in Lattice Fields*, *Adv. Phys.* **3**, 325 (1954).
- [23] J. Tempere, W. Casteels, M. K. Oberthaler, S. Knoop, E. Timmermans, and J. T. Devreese, *Feynman Path-Integral Treatment of the BEC-Impurity Polaron*, *Phys. Rev. B* **80**, 184504 (2009).
- [24] F. Grusdt, Y. E. Shchadilova, A. N. Rubtsov, and E. Demler, *Renormalization Group Approach to the Fröhlich Polaron Model: Application to Impurity-BEC Problem*, *Sci. Rep.* **5**, 12124 (2015).
- [25] T. Yin, D. Cocks, and W. Hofstetter, *Polaronic Effects in One- and Two-Band Quantum Systems*, *Phys. Rev. A* **92**, 063635 (2015).
- [26] In all the experiments, the gases are spin polarized in the absolute hyperfine ground state.
- [27] T. Schuster, R. Scelle, A. Trautmann, S. Knoop, M. K. Oberthaler, M. M. Haverhals, M. R. Goosen, S. J. J. M. F. Kokkelmans, and E. Tiemann, *Feshbach Spectroscopy and Scattering Properties of Ultracold Li + Na Mixtures*, *Phys. Rev. A* **85**, 042721 (2012).

- [28] L. Khaykovich, F. Schreck, G. Ferrari, T. Bourdel, J. Cubizolles, L. D. Carr, Y. Castin, and C. Salomon, *Formation of a Matter-Wave*, *Science* **296**, 1290 (2002).
- [29] The excitation efficiency is limited by residual atoms in the excited state at the beginning of the experiment and by a weak coupling of the second excited state which is suppressed by the anharmonicity of the potential.
- [30] A. Kastberg, W. D. Phillips, S. L. Rolston, R. J. C. Spreeuw, and P. S. Jessen, *Adiabatic Cooling of Cesium to 700 nK in an Optical Lattice*, *Phys. Rev. Lett.* **74**, 1542 (1995).
- [31] M. Greiner, I. Bloch, O. Mandel, T. W. Hänsch, and T. Esslinger, *Exploring Phase Coherence in a 2D Lattice of Bose-Einstein Condensates.*, *Phys. Rev. Lett.* **87**, 160405 (2001).
- [32] I. Bloch, J. Dalibard, and W. Zwerger, *Many-Body Physics with Ultracold Gases*, *Rev. Mod. Phys.* **80**, 885 (2008).
- [33] Each Ramsey fringe is sampled at 10 points. One series of measurements consists of at least three samplings of the whole fringe. For each repetition the scans with and without BEC present are separately fitted with a sine function and the final value for the phase shift is calculated as a weighted mean of the repetitions. Shots with extreme atom numbers, deviating lattice intensity, or at wrong wavelength are discarded. If several measurement series can be combined, their result is calculated as the weighted mean of the individual values.
- [34] S. Knoop, T. Schuster, R. Scelle, A. Trautmann, J. Appmeier, M. K. Oberthaler, E. Tiesinga, and E. Tiemann, *Feshbach Spectroscopy and Analysis of the Interaction Potentials of Ultracold Sodium*, *Phys. Rev. A* **83**, 042704 (2011).
- [35] S. P. Rath and R. Schmidt, *Field-Theoretical Study of the Bose Polaron*, *Phys. Rev. A* **88**, 053632 (2013).
- [36] F. Grusdt, A. Shashi, D. Abanin, and E. Demler, *Bloch Oscillations of Bosonic Lattice Polarons*, *Phys. Rev. A* **90**, 063610 (2014).
- [37] A. Shashi, F. Grusdt, D. A. Abanin, and E. Demler, *Radio-Frequency Spectroscopy of Polarons in Ultracold Bose Gases*, *Phys. Rev. A* **89**, 053617 (2014).
- [38] F. Grusdt and E. Demler, in *Quantum Matter at Ultralow Temperatures*, edited by M. Inguscio, W. Ketterle, S. Stringari, and G. Roati (IOS Press, Amsterdam, 2016).
- [39] G. D. Mahan, *Many-Particle Physics*, 3rd ed. (Springer, New York, 2000) pp. XII, 785.
- [40] A similar discussion for the electronic levels around ionic impurities in semiconductors is presented in Ref. [41].
- [41] B. A. Mason and S. Das Sarma, *Phonon-Induced Shift in Shallow Donor Levels of Semiconductor Quantum Structures*, *Phys. Rev. B* **33**, 8379 (1986).
- [42] For very large values of  $\eta$  we excite approximately 10% of the atoms into the third band. They are not taken into account in our analysis as they experience only a negligible energy shift compared to atoms in the lower two states.
- [43] I. Bloch, J. Dalibard, and S. Nascimbène, *Quantum Simulations with Ultracold Quantum Gases*, *Nat. Phys.* **8**, 267 (2012).
- [44] P. A. Lee, *From High Temperature Superconductivity to Quantum Spin Liquid: Progress in Strong Correlation Physics*, *Rep. Prog. Phys.* **71**, 012501 (2008).
- [45] A. Recati, J. N. Fuchs, C. S. Peca, and W. Zwerger, *Casimir Forces between Defects in One-Dimensional Quantum Liquids*, *Phys. Rev. A* **72**, 023616 (2005).
- [46] M. Schechter and A. Kamenev, *Phonon-Mediated Casimir Interaction between Mobile Impurities in One-Dimensional Quantum Liquids*, *Phys. Rev. Lett.* **112**, 155301 (2014).
- [47] A. Klein and M. Fleischhauer, *Interaction of Impurity Atoms in Bose-Einstein Condensates*, *Phys. Rev. A* **71**, 033605 (2005).
- [48] J. N. Fuchs, A. Recati, and W. Zwerger, *Oscillating Casimir Force between Impurities in One-Dimensional Fermi Liquids*, *Phys. Rev. A* **75**, 043615 (2007).
- [49] C. M. Wilson, G. Johansson, A. Pourkabirian, J. R. Johansson, T. Duty, F. Nori, and P. Delsing, *Observation of the Dynamical Casimir Effect in a Superconducting Circuit*, *Nature (London)* **479**, 376 (2011).
- [50] T. Ramos, H. Pichler, A. J. Daley, and P. Zoller, *Quantum Spin Dimers from Chiral Dissipation in Cold-Atom Chains*, *Phys. Rev. Lett.* **113**, 237203 (2014).
- [51] M. G. Hu, M. J. Van de Graaff, D. Kedar, J. P. Corson, E. A. Cornell, and D. S. Jin, *Bose Polarons in the Strongly Interacting Regime*, *Phys. Rev. Lett.* **117**, 055301 (2016).
- [52] N. B. Jørgensen, L. Wacker, K. T. Skalmstang, M. M. Parish, J. Levinsen, R. S. Christensen, G. M. Bruun, and J. J. Arlt, *Observation of Attractive and Repulsive Polarons in a Bose-Einstein Condensate*, *Phys. Rev. Lett.* **117**, 055302 (2016).